IJMMM International Journal of Minerals, Metallurgy and Materials 矿物冶金与材料学报（英文版）

Exploring the potential of olivine-containing copper–nickel slag for carbon dioxide mineralization in cementitious materials

Qianqian Wang, Zequn Yao, Lijie Guo, and Xiaodong Shen

Cite this article as:
Qianqian Wang, Zequn Yao, Lijie Guo, and Xiaodong Shen, Exploring the potential of olivine-containing copper–nickel slag for carbon dioxide mineralization in cementitious materials, *Int. J. Miner. Metall. Mater.*, 31(2024), No. 3, pp. 562-573. https://doi.org/10.1007/s12613-023-2743-1

Articles you may be interested in

Dawei Yu and Kinnor Chattopadhyay, Enhancement of the nickel converter slag-cleaning operation with the addition of spent potlining, *Int. J. Miner. Metall. Mater.*, 25(2018), No. 8, pp. 881-891. https://doi.org/10.1007/s12613-018-1637-0

Rong Zhu, Bao-chen Han, Kai Dong, and Guang-sheng Wei, A review of carbon dioxide disposal technology in the converter steelmaking process, *Int. J. Miner. Metall. Mater.*, 27(2020), No. 11, pp. 1421-1429. https://doi.org/10.1007/s12613-020-2065-5

Hua-zhe Jiao, Shu-fei Wang, Ai-xiang Wu, Hui-ming Shen, and Jian-dong Wang, Cementitious property of $NaAlO_2$-activated Ge slag as cement supplement, *Int. J. Miner. Metall. Mater.*, 26(2019), No. 12, pp. 1594-1603. https://doi.org/10.1007/s12613-019-1901-y

Zhong-qing Liu, Jian Zheng, Yi Wang, and Xu Liu, Selective reduction of carbon dioxide into amorphous carbon over activated natural magnetite, *Int. J. Miner. Metall. Mater.*, 28(2021), No. 2, pp. 231-237. https://doi.org/10.1007/s12613-020-2034-z

Qing Yuan, Guang Xu, Wei-cheng Liang, Bei He, and Ming-xing Zhou, Effects of oxygen content on the oxidation process of Si-containing steel during anisothermal heating, *Int. J. Miner. Metall. Mater.*, 25(2018), No. 2, pp. 164-172. https://doi.org/10.1007/s12613-018-1559-x

Hamed Jamshidi Aval, Microstructural evolution and mechanical properties of friction stir-welded C71000 copper-nickel alloy and 304 austenitic stainless steel, *Int. J. Miner. Metall. Mater.*, 25(2018), No. 11, pp. 1294-1303. https://doi.org/10.1007/s12613-018-1682-8

IJMMM WeChat

QQ author group

INTERNATIONAL JOURNAL OF
Minerals, Metallurgy and Materials

Volume 31, Number 3, March 2024
Page 562

Research Article https://doi.org/10.1007/s12613-023-2743-1

Exploring the potential of olivine-containing copper–nickel slag for carbon dioxide mineralization in cementitious materials

Qianqian Wang[1,2),✉], *Zequn Yao*[1,2)], *Lijie Guo*[3),✉], *and Xiaodong Shen*[1,2)]

1) College of Materials Science and Engineering, Nanjing Tech University, Nanjing 211816, China
2) State Key Laboratory of Materials-Oriented Chemical Engineering, Nanjing 211816, China
3) BGRIMM Technology Group, Beijing 100160, China
(Received: 10 May 2023; revised: 10 September 2023; accepted: 12 September 2023)

Abstract: Water-quenched copper-nickel metallurgical slag enriched with olivine minerals exhibits promising potential for the production of CO_2-mineralized cementitious materials. In this work, copper-nickel slag-based cementitious material (CNCM) was synthesized by using different chemical activation methods to enhance its hydration reactivity and CO_2 mineralization capacity. Different water curing ages and carbonation conditions were explored related to their carbonation and mechanical properties development. Meanwhile, thermogravimetry differential scanning calorimetry and X-ray diffraction methods were applied to evaluate the CO_2 adsorption amount and carbonation products of CNCM. Microstructure development of carbonated CNCM blocks was examined by backscattered electron imaging (BSE) with energy-dispersive X-ray spectrometry. Results showed that among the studied samples, the CNCM sample that was subjected to water curing for 3 d exhibited the highest CO_2 sequestration amount of 8.51wt% at 80°C and 72 h while presenting the compressive strength of 39.07 MPa. This result indicated that 1 t of this CNCM can sequester 85.1 kg of CO_2 and exhibit high compressive strength. Although the addition of citric acid did not improve strength development, it was beneficial to increase the CO_2 diffusion and adsorption amount under the same carbonation conditions from BSE results. This work provides guidance for synthesizing CO_2-mineralized cementitious materials using large amounts of metallurgical slags containing olivine minerals.

Keywords: copper–nickel slag; fayalite; CO_2 sequestration; cementitious material; admixtures; carbonation conditions

1. Introduction

Global annual carbon emissions reached a new high of over 36.8 Gt in 2022 [1], increasing by approximately 1.9 Gt relative to those in 2021 [2]. Alkaline solid wastes are suitable for CO_2 mineralization due to their high reactivity and intrinsic alkalinity [3–7]. However, these solid wastes normally require activation to adsorb CO_2. Using large amounts of alkaline solid wastes with low cement contents to prepare CO_2-mineralized cementitious materials can be a mild and cost-effective way for their large-scale application.

However, two technical bottlenecks exist in improving the carbonation efficiency of solid wastes made of cementitious materials: new ways to enhance the dissolution efficiency of olivine or other alkaline minerals and physical parameters during carbonation. Using different types of organic acids to form alkaline metal ion chelates [8–10] could be a way to improve the metal ion content of solid wastes, which is important for enhancing their reactivity with CO_2. Researchers [11–15] have investigated the dynamics of solid–liquid–gas reactions by varying the pressure and state of CO_2 (such as the supercritical state), the particle size and pH of solids or pastes, the humidity levels of carbonation reactors and the time and temperature of the reaction. They aim to identify the accelerating conditions and limiting steps during carbonation [10]. These fundamental works guide not only CO_2 mineralization in mineral ores but also the carbonation of solid wastes for the preparation of supplementary cementitious materials (SCMs) or binders, including steel slag [16], magnesium slag [17], cement kiln dust and reactive MgO [18].

Nickel extraction mine tailings or metallurgical slags have recently been taken as sources of alkaline wastes for carbon mineralization [7,9]. Mineral composition analysis has revealed that nickel slag contains abundant crystalline olivine phases that are isolated silicate tetrahedrons composed of divalent cations, such as Ca, Mg and, Fe [19–20]. Early studies have shown that these olivine phases are abundantly distributed in the crustal surface worldwide. Their carbonation efficiency is high, and their resulting carbonate products are thermodynamically stable. The annual output of nickel slag is approximately 4 million t, but the utilization rate of nickel slag is less than 10% worldwide [21–23]. Water-quenched nickel slag contains some amorphous phases that can potentially be used as SCMs [24–26]. Given these two points, preparing CO_2-mineralized cementitious materials by using nickel slag may be highly promising [27–28]. However, the CO_2

✉ Corresponding authors: Qianqian Wang E-mail: qqwang@njtech.edu.cn; Lijie Guo E-mail: guolijie@bgrimm.com

mineralization efficiency and mechanical properties of composite cementitious materials made from olivine-rich copper–nickel metallurgical slag have not been studied before.

In this work, copper–nickel slag was applied as the main metallurgical slag to synthesize composite cementitious materials for CO_2 mineralization. Chemical additives, such as citric acid (CA), were used to increase the reactivity and dissolution rate of copper-nickel slag. P II 52.5 cement and water glass were utilized as alkaline binders. The synthesized copper-nickel slag-based cementitious material (CNCM) was composed of 80wt% activated copper-nickel slag and 20wt% cement. Paste blocks made with CNCM were pre-cured at different ages and then carbonated at different carbonation temperatures and times under 70%–80% relative humidity (RH). The mechanical properties, carbonated products, CO_2 adsorption content (CAC) and microstructure development of the carbonated blocks were further studied and analyzed. This work could be a guide for synthesizing CO_2-mineralized cementitious materials with large amounts of metallurgical slags.

2. Experimental

2.1. Raw materials

The copper–nickel slag and cement used in this study were from the same batch of raw materials used in a previous study [29] and are shown in Fig. S1 and Table S1 in Supplementary Materials (SM). The main phase of copper–nickel slag was fayalite, with a median particle size of 15.15 μm. The chemical composition of copper-nickel slag was mainly Fe_2O_3, SiO_2, MgO, and a small amount of Al_2O_3 and CaO. The chemical admixtures used in this study were water glass with a modulus of 1.5 and analytically pure citric acid (CA) from Aladdin, Shanghai.

2.2. Experimental methods

The preparation and carbonation of CNCM consisted of three stages, as shown in Fig. 1. First, the raw copper-nickel slag was pretreated through different methods to synthesize CNCM. The mix design of the copper–nickel slag composite cementitious material is shown in Table 1. Sample B was a blank sample with only 20wt% cement. Sample D was a reference sample with 9wt% water glass and 20wt% cement. Sample CA was a sample pretreated with 0.3 mol/L CA and then mixed with 9wt% water glass and 20wt% cement. Subsequently, the blocks that were synthesized with different types of CNCM were water-cured for different ages at 20°C. Before carbonation, the blocks were pre-dried at 25°C for 12 h until their surfaces were dry. In the accelerated carbonation reaction stage, the test blocks were placed in a carbonation reactor wherein the humidity was maintained at >60%. CO_2 with 99.9vol% was injected into the reactor until the reactor reached 1 MPa. The carbonation temperature was set at 35 or 80°C, and the curing ages were 24 or 72 h.

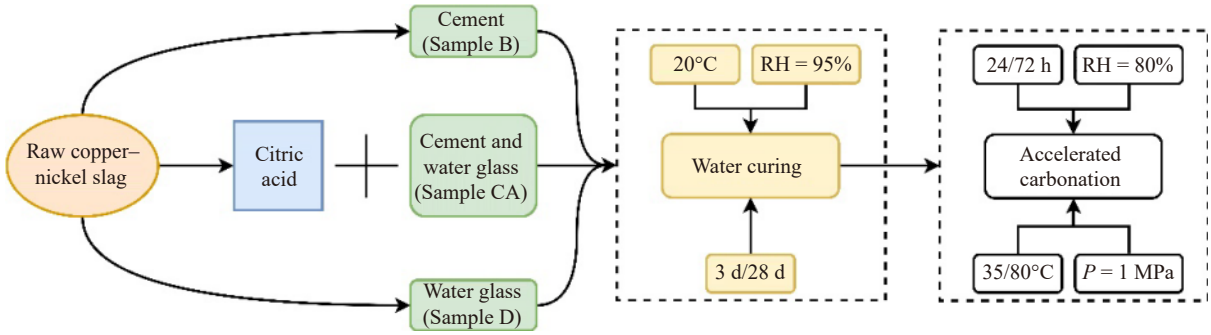

Fig. 1. Preparation of CNCM. Here, Sample B was a blank sample with only 20wt% cement. Sample D was a reference sample with 9wt% water glass and 20wt% cement. Sample CA was a sample pretreated with 0.3 mol/L CA and then mixed with 9wt% water glass and 20wt% cement. *P*: the pressure of carbon dioxide.

Table 1. Ratio design of CNCM

Sample	Slag / wt%	Portland cement / wt%	Admixture / (mol·L^{-1})	$Na_2O{\cdot}nSiO_2$ modulus	Water glass / wt%	Water to cement mass ratio
B			—		—	
D	80	20	—	1.5	9	0.23
CA			0.3 mol/L		—	

2.3. Test and characterization methods

The compressive strength of the test blocks in each set of specimens was tested before and after carbonation. The carbonation properties and microstructures of the CNCM samples obtained under different carbonation conditions were characterized through X-ray diffraction (XRD), thermogravimetry–differential scanning calorimetry (TG–DSC), mercury intrusion porosimetry (MIP), and backscattered electron imaging (BSE) with energy dispersive X-ray spectrometry (EDS). All the test and characterization parameters are listed in the SM in detail.

Furthermore, the CO_2 adsorption content (CAC) was calculated by using Eq. (1). The mass difference Δw_1 was extracted from the TG curves of the carbonated CNCM samples

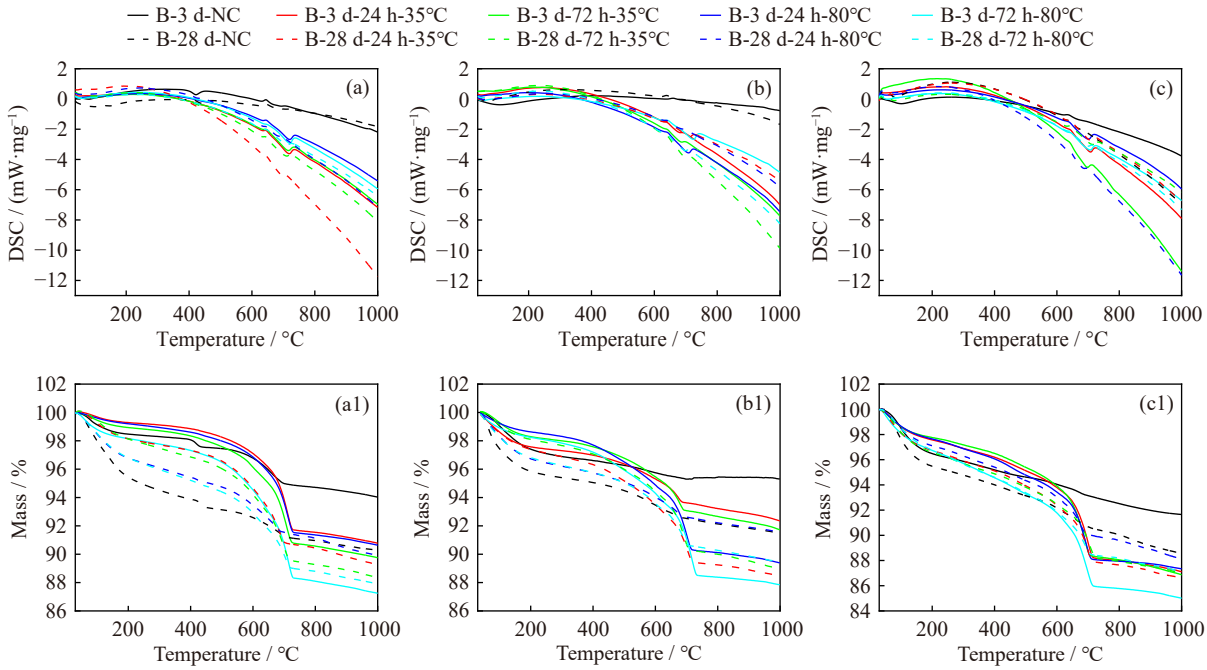

Fig. 2. DSC (a–c) and TG (a_1–c_1) curves of CNCM at 35 and 80°C after 24 and 72 h of CO_2 curing.

at 550–750°C in reference to those of uncarbonated samples, as shown in Fig. 2.

$$\text{CAC (wt\%)} = \frac{\Delta w_1}{\text{Initial mass}} \tag{1}$$

where Δw_1 represents the content of carbonated products after carbonation. Initial mass refers to the mass of the dried samples of carbonated CNCM.

The mass variations of the samples before and after carbonation were calculated by using Eq. (2), where m_0 and m_1 represent the mass of the block before and after carbonation, respectively.

$$\text{Mass variation} = \frac{m_1 - m_0}{m_0} \tag{2}$$

The percentage of porosity reduction (V_r) is calculated as follows:

$$V_r = \frac{V_C - V_{NC}}{V_C} \tag{3}$$

where V_r represents the magnitude of porosity reduction, V_C represents the total porosity of the carbonated sample, and V_{NC} represents the porosity of uncarbonated samples.

3. Results and discussion

3.1. CAC from TG–DSC

Fig. 2 shows the TG/DSC curves of the CNCM samples before and after the accelerated carbonation reaction. The DSC peaks at 400, 650, and 700°C corresponded to the endothermic peak of $Ca(OH)_2$ (CH) decomposition, the exothermic peak of the oxidation of a small amount of Fe^{2+} in copper–nickel slag into Fe^{3+}, and the endothermic peaks of carbonate decomposition, respectively. Fig. 2 shows that samples B, D, and CA presented the highest carbonation product contents after 3 d of water curing at 80°C and 72 h. The TG curves illustrate that after 28 d of water curing, sample B presented its maximum weight loss at 80°C and 72 h, whereas samples D and CA exhibited their maximum weight losses at 35°C and 24 h, indicating that more carbonated products formed in the cementitious materials than in the other materials. In addition, the test blocks that were water-cured for 3 d produced more carbonated products than the test blocks that were water-cured for 28 d.

Fig. 3 shows the CAC columns of the CNCM samples after carbonation. Fig. 3(a) illustrates that the CACs of different samples carbonated at 35°C after 3 d of water curing were mainly related to the mixing design of CNCM instead of the CO_2 curing time. Sample D had the lowest CAC among the three samples. The CACs of different samples did not significantly differ after 28 d of water curing.

Fig. 3(b) illustrates that the CAC of different samples carbonated at 80°C was mainly related to water curing ages and CO_2 curing times. The CACs of the samples water-cured for 3 d were almost twice those of the samples water-cured for 28 d. After the CO_2 curing time was extended from 24 h to 72 h, the average increment rate of the CACs of all the samples exceeded 30%. The effect of mixing design on CAC was observable only in the samples water-cured for 28 d and subjected to 72 h of CO_2 curing.

By comparing the data in Fig. 3(a) and (b), it revealed that carbonation temperature mainly influenced the CACs of the samples water-cured for 28 d, i.e., the CACs of the samples at 80°C decreased relative to those at 35°C. On the contrary, the CAC of sample D was approximately twice that of the sample in the case wherein the carbonation temperature increased from 35 to 80°C. The reason could be: that a high carbonation temperature accelerated the diffusion of CO_2 in the condensed pastes in the water glass-activated hydration products, such as early C(N)–S–H gels [30].

Water curing for long durations, i.e., 28 d, increased the hydration degree of the CNCM samples and decreased

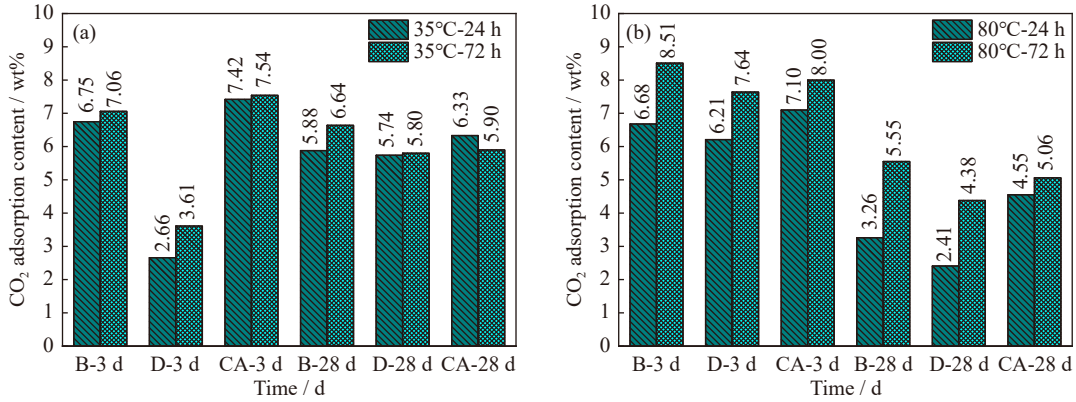

Fig. 3. Columns of the CACs of the CNCM samples after carbonation under different conditions: (a) 35°C; (b) 80°C.

porosity, hindering CO_2 diffusion and decreasing the carbonization degree. However, a short period of water curing did not considerably improve the density of the system such that the diffusion of CO_2 was relatively facilitated, resulting in a higher degree of carbonization.

In general, a high temperature, i.e., 80°C, was beneficial to CO_2 adsorption and carbonization depth (the profile map of the carbonized blocks is shown in Fig. S2) in different CNCM types subjected to 3, instead of 28 d of water curing [31]. At 80°C, CO_2 diffusion in the test blocks was accelerated, leading to the increased dissolution of metal cations from the olivine phase to produce additional carbonation products and increase CO_2 adsorption. In this case, extending the CO_2 curing time further increased CACs by accelerating CO_2 diffusion [32]. Sample B, subjected to 3 d of water curing, exhibited the highest CAC value of 8.51wt% under the specific conditions of 80°C carbonation temperature and 72 h carbonation time, which indicated that 1 t of this copper-nickel slag composite cementitious material can sequester 85.1 kg of CO_2.

3.2. Mass variation of samples before and after carbonation

Fig. 4 shows the mass variation of the CNCM samples before and after carbonation. Among the samples, sample B, subjected to 3 d of water curing, showed the highest mass increment of 3.39% after carbonation at 35°C for 72 h. After 3 d of pre-curing, sample D showed the lowest mass variation, which was consistent with its lowest CAC. Under the conditions of 35°C and 72 h and 80°C and 24 h, sample CA also had a higher mass variation than other test blocks except for sample B. After 28 d of pre-curing, sample D showed the highest percent change in mass, whereas samples CA and B had low mass variations under carbonation at 35°C. Samples D and CA presented a lower mass variation at 80°C than at 35°C, and the mass variation of sample B did not considerably improve with the extension of time.

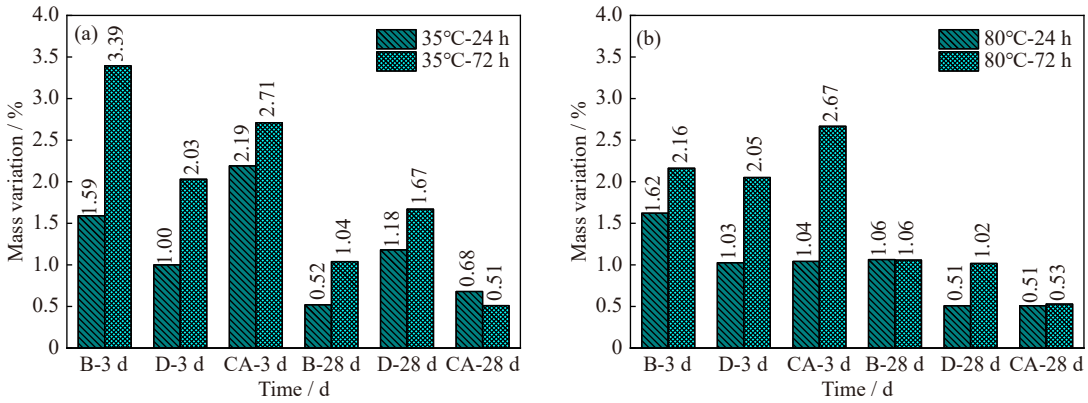

Fig. 4. Mass variation of the CNCM samples before and after carbonation.

The mass change of the CNCM samples due to carbonation was consistent with the trend of CACs shown in Fig. 3. Regardless of carbonation temperature and mixing design, the samples cured for 3 d had high mass increments after different carbonation times. The mass increment of the samples that were water-cured for 28 d was less than 1.67% after different carbonation times.

Generally, both water curing age and carbonation time are the most significant factors influencing the mass variation of the samples after carbonation. In the 3 d water curing samples, their higher porosity could account for their largely improved water adsorption content and CO_2 diffusion and adsorption amounts.

It should be noted that the mass variation depended largely on system porosity because the water saturation method was used for mass weighing. Therefore, the mass variation of the

test blocks after carbonization may have varied under different conditions. Moreover, some carbonic acid that may exist in the test blocks was released in the form of CO_2 during water saturation. This process also affected the mass variation.

3.3. Phase change after carbonation from XRD analysis

Fig. 5 shows the XRD patterns of all the CNCM samples before and after carbonation. Before carbonation, the main phases in the hydrated CNCM were fayalite, Fe_3O_4, CH, unhydrated C_3S and C_2S. Samples D and CA had lower fayalite and CH contents than sample B after 3 and 28 d of water curing. After carbonation, aragonite, calcite, and vaterite showed different peak intensities, with the peak intensity of CH showing a reduction.

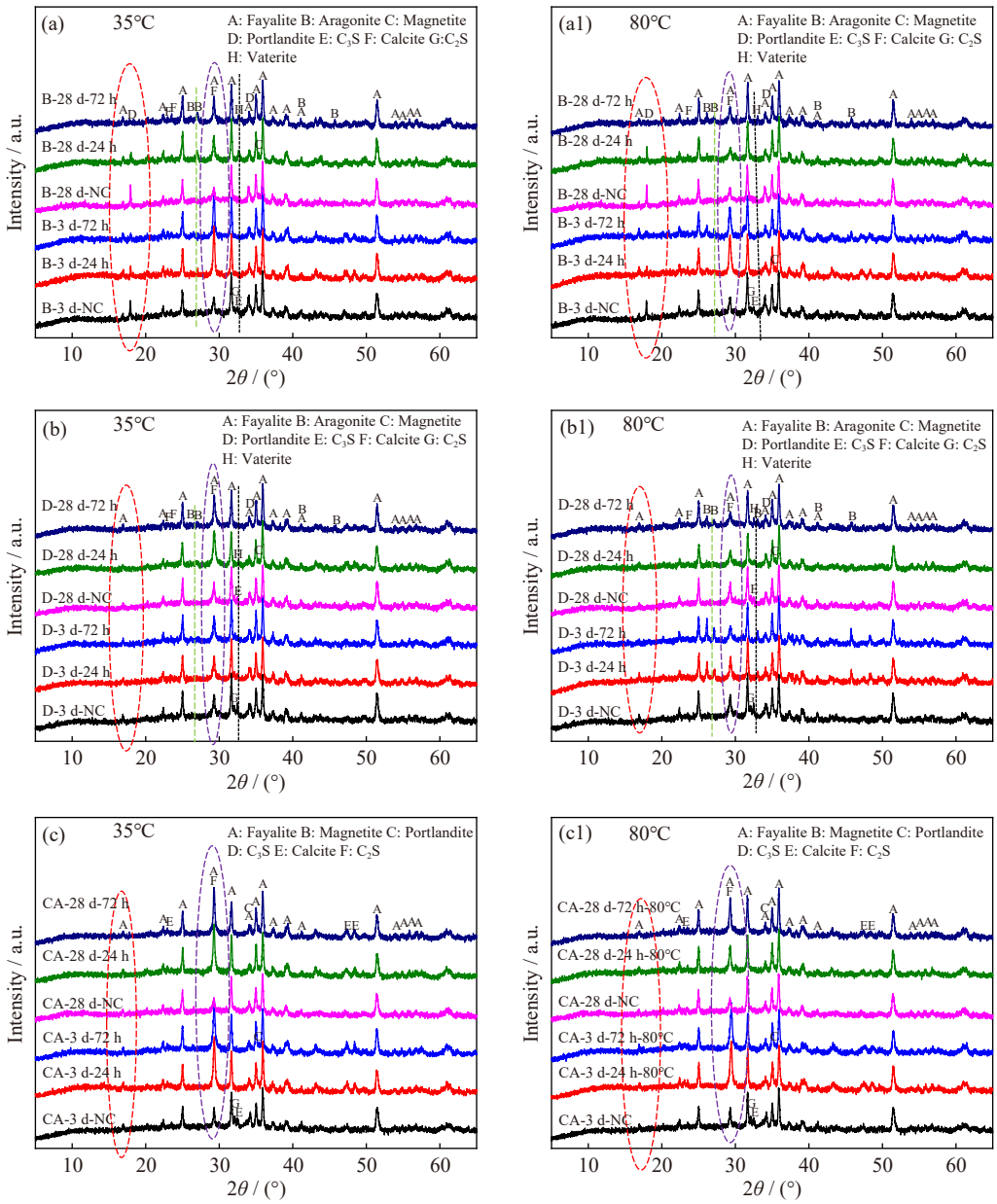

Fig. 5. XRD patterns of CNCM samples water-cured for 3 and 28 d after CO_2 adsorption at (a–c) 35°C and (a1–c1) 80°C for 24 and 72 h, respectively. Red ovals represent the peak intensity variation of CH and fayalite; blue ovals indicate the content variation of calcite; green dashed lines indicate the peak of aragonite; and gray dashed lines indicate the peak of vaterite.

The different mixing designs of CNCM, i.e., chemical activation methods, were the main factor influencing $CaCO_3$ polymorphs. For example, only calcite was observed in sample CA, whereas all polymorphs of $CaCO_3$, such as calcite, aragonite, and vaterite, were found in samples D and B. Although carboxylic acid groups do not affect the nucleation of $CaCO_3$, they can influence the polymorph of $CaCO_3$ by adsorbing $CaCO_3$ on organic acid particles. Metal ions, such as Mg^{2+}, can cause the crystal lattice distortion of calcium carbonate and promote its transformation into calcite-type calcium carbonate. Carboxylic acid groups also enhanced the dissolution of fayalite and forsterite in copper-nickel slag and released some metal cations, resulting in the predominance of calcite as the crystal form of calcium carbonate [33].

Water curing age and carbonation temperature also re-

markably affected the change in $CaCO_3$ polymorphs. After 28 d of water curing, vaterite was more easily observed in sample D or B than in other samples. With the increase in carbonation temperature, the formation of aragonite and vaterite was facilitated. Previous studies have indicated that a high reaction temperature favors the formation of aragonite [34]. However, carbonation time can only increase carbonate content. The above results show that carbonation time could not change the $CaCO_3$ polymorphs in the carbonated samples.

In general, the increment in the peak intensity of carbonates corresponded to the CACs extracted from the TG–DSC results shown in Fig. 3. Carbonation is mostly affected by the reaction temperature, which influences the diffusion–adsorption of CO_2 in the test block, the dissolution of cations in copper-nickel slag [31], and the change in $CaCO_3$ polymorphs. As the temperature increased, the change in polymorphs became increasingly apparent. Additionally, the mixing design can result in different diffraction peaks and polymorph changes in the carbonation products of the CNCM samples. For instance, the addition of water glass changed the original pH value of the hardened paste, increasing the content of aragonite and vaterite. Thus, the system of aragonite, calcite, and aragonite formed [35].

In addition, fayalite can be dissolved in acidic or basic solutions [8]. This work confirmed that the peak intensity of fayalite in all three samples decreased. A previous study found that after fayalite dissolved, siderite formed in water-saturated supercritical CO_2 [11]. However, we did not find the formation of siderite in these carbonation conditions in this work. This result also implied that the carbonation condition had a significant impact on carbonation phase formation and carbonate polymorphs.

3.4. Compressive strength of carbonated CNCM samples

The average compressive strengths of the three blocks before and after carbonation are shown in Fig. 6. Before carbonation, the compressive strength of the CNCM samples considerably differed with different chemical additives. Sample D, activated with water glass subjected to 3 d of water curing, exhibited the highest compressive strength (12.85 MPa), whereas sample CA activated with citric acid had negligible compressive strength. This could be attributed that the COOH groups retarded its hydration reaction and increased its porosity [36]. After 28 d of water curing without chemical activation, sample B showed the highest compressive strength (36.05 MPa), whereas sample CA continued to show the lowest.

The compressive strength of the samples increased significantly after carbonation. Especially, after 3 d of water curing, the carbonated sample CA showed the highest compressive strength increases of approximately 20 MPa among the three CNCM samples. Sample B showed the smallest increase in compressive strength regardless of the carbonation temperature (35 or 80°C). However, after 28 d of water curing at 35 or 80°C, sample CA, presented the lowest compressive strength among the three CNCM samples, followed by sample D.

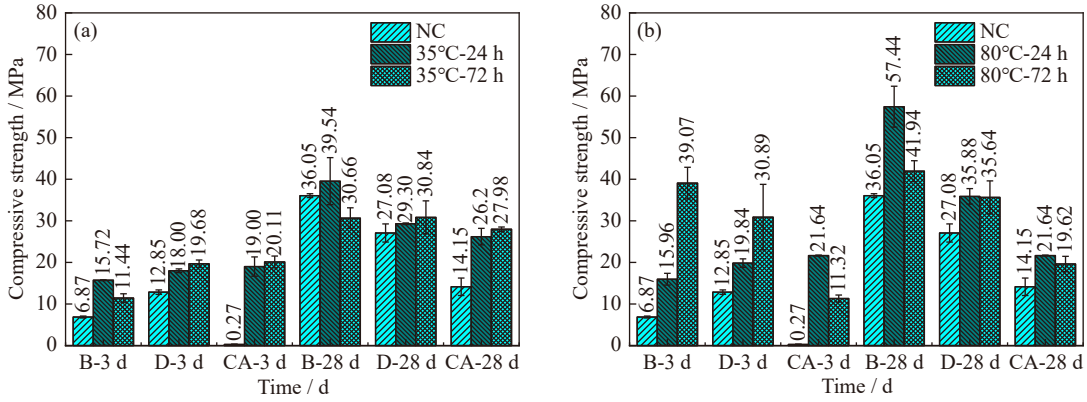

Fig. 6. Compressive strengths of the CNCM samples before and after carbonation under different conditions corresponding to the samples in Fig. 5: (a) 35°C; (b) 80°C. NC means the condition of non-carbonation.

After carbonation for 72 h at 35°C, sample CA, subjected to 3 d of water curing, exhibited the highest compressive strength among the three CNCM samples, followed by sample D. The three CNCM samples subjected to 28 d of water curing and carbonated at 35°C showed similar compressive strengths. Sample CA had the lowest compressive strength among the three CNCM samples carbonated at 80°C regardless of water curing ages, while it had higher compressive strength when carbonated at 35°C. In general, the compressive strengths of samples B and D increased as a result of increasing the carbonation temperature from 35 to 80°C. Sample B had the highest compressive strength, 57.44 MPa, among the three CNCM samples carbonated at 80°C.

When the carbonation time increased from 24 to 72 h, only six samples showed improved compressive strength, five samples presented reduced compressive strength, and the compressive strength of one sample remained the same. The increase in strength, particularly that observed when the carbonation time was 24 h, can be attributed to the synergistic effect of hydration and carbonation. As time passed, hydration products accumulated in the system, whereas carbonation products gradually formed in pores during low-temperature accelerated carbonization [37]. Carbonating the samples at 80°C and extending the carbonation time can en-

hance CO_2 diffusion and generate excessive carbonation products that fill pores. However, this process can also lead to the destruction of hydration products, including C–S–H [38–39].

3.5. Microstructure development of carbonated CNCM

3.5.1. MIP

Fig. 7 shows the pore structure of the CNCM samples subjected to 28 d of water curing before and after carbonation. Fig. 8 depicts the total intruded volume and total porosity of the samples subjected to 28 d of water curing before and after carbonation.

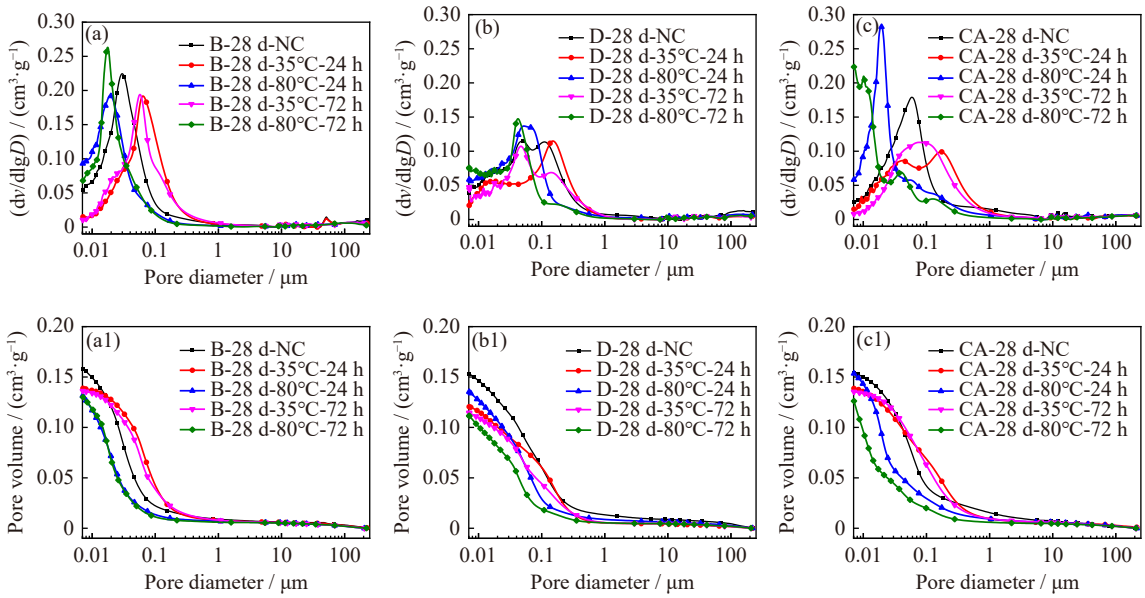

Fig. 7. Pore structure of CNCM blocks subjected to 28 d of water curing before and after CO_2 adsorption: (a, b, c) pore size distribution and (a_1, b_1, c_1) cumulative pore volume.

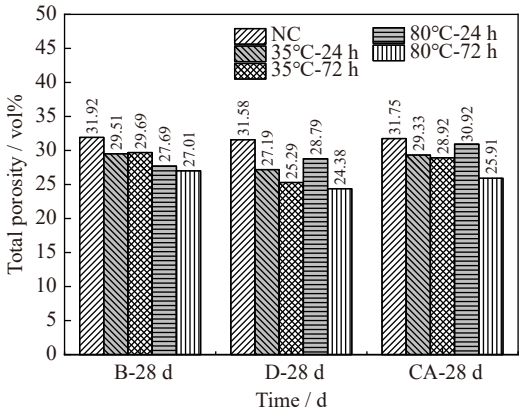

Fig. 8. Total porosity of samples B, D, and CA after 28 d of water curing before and after carbonation.

The peak value of the pore size distribution of all the samples was less than 1 μm. In general, carbonation temperature is the key factor modifying the main peak value of pore size distribution: compared to the uncarbonated samples at the same carbonation temperature, 35°C shifted the main peak value to the large region, and 80°C shifted the main peak value to the small region. Furthermore, extending the carbonation time from 24 to 72 h at the same carbonation temperature shifted the main peak value to the small region. This result suggested that reasonable carbonation conditions can refine the pore structures of the hardened pastes.

Previous work found that cement paste cured at 60°C showed increased porosity and pore size [31]. However, in the present work, the total porosity of all the samples decreased considerably after carbonation, as shown in Fig. 8. Specifically, the porosities of samples B, D and CA decreased by 7%–15%, 8%–23%, and 3%–19% (calculated according to Eq. (3)), respectively, implying that the formation of carbonates decreased total porosity while changing pore distribution. This result showed that the filling effect of carbonation products improved pore structure [40]. Sample D had a broad pore reduction range, likely because a high carbonization temperature led to increases in hydration reactions [41].

The results in Fig. 8 indicate that the total porosity of the sample carbonized at 35°C for 24 and 72 h gradually decreased in line with the increase in strength observed in Fig. 6. For the samples carbonized at 80°C, the total porosity of sample D corresponded to the development of compressive strength. Sample CA showed higher porosity after 24 h of carbonization than after 72 h of carbonization but poorer compressive strength after 72 h of carbonization than after 24 h of carbonization. This inconsistency could be attributed to the destruction of hydration products by excessive carbonization, causing the initial part of the dense structure to expand and leading to a reduction in strength.

After 28 d of water curing, sample D showed a lower peak value and cumulative volume of main pore size distribution than sample B. Sample CA had a slightly larger pore size before carbonation but a similar pore development trend as sample B after carbonation. This result suggested that sodium silicate reduced early porosity by enhancing bonding and

hydration. This effect led to low carbon adsorption amounts under the same carbonation conditions. CA increased the porosity of the system, resulting in a high carbon adsorption amount. This result further indicates that large pore sizes or increases in pores can effectively increase carbon sequestration [38].

3.5.2. BSE and EDS

The BSE images of samples B, D, and CA cured for 28 d before and after carbonation are shown in Figs. 9,10 and 11, respectively. Fig. 9 shows that before carbonation, a large amount of fayalite with numerous pores and low structural continuity was present, resulting in a relatively loose structure. After carbonation at 35°C, the hardened paste of sample B became filled with additional carbonation products, increasing paste continuity. The continuity of the hardened paste of sample B carbonated at 80°C further enhanced compared with that of the samples carbonated at 35°C. This effect corresponded to the decrease in total porosity shown in Fig. 8.

Fig. 9(c) illustrates that cracks or dissolution steps were present on the fayalite surface before carbonation. Fig. 9(c_1) and (c_2) shows that after carbonation at different temperatures, i.e., 35 or 80°C, the particle diameter of fayalite decreased. In particular, one fayalite particle decomposed and a new phase formed inside the cracks after carbonation.

Fig. 10 shows that sample D experienced minor micro-

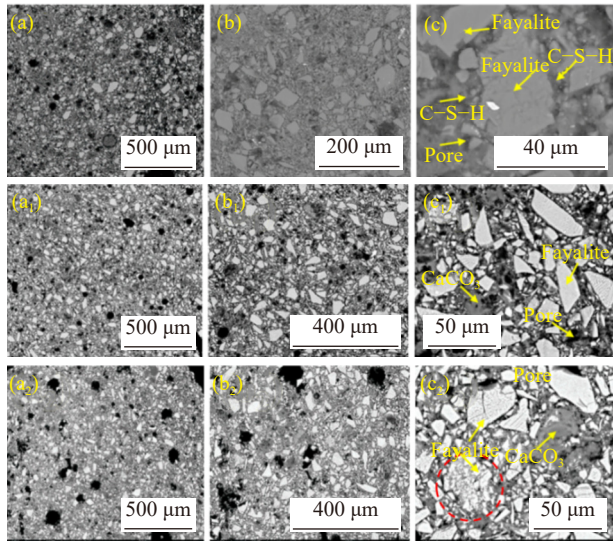

Fig. 9. (a, b, c) BSE images of sample B subjected to 28 d of water curing and carbonated at (a_1, b_1, c_1) 35°C and (a_2, b_2, c_2) 80°C for 24 h. The red circle represents decomposed fayalite particles with the formation of a new phase.

structural changes and particle diameter reduction after carbonation. Therefore, the compressive strength of sample D after 24 h of carbonation at 35°C slightly increased, likely because the high degree of hydration in the early stage led to the reduction in the degree of carbonization and water glass

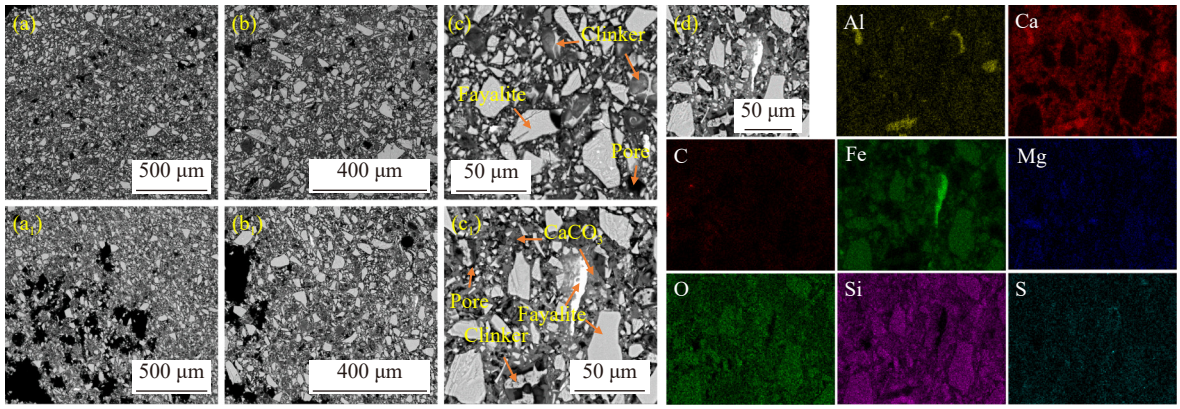

Fig. 10. BSE images of sample D without carbonation (a, b, c) and with carbonation at 35°C (a_1, b_1, c_1) and (d) EDS images of sample D (subjected to 28 d of water curing).

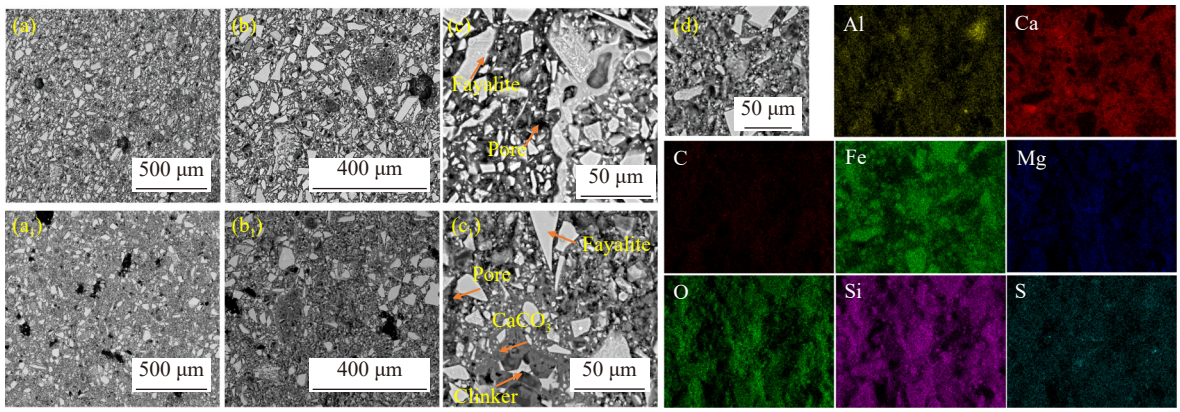

Fig. 11. BSE images of sample CA without carbonation (a, b, c) and with carbonation at 35°C (a_1, b_1, c_1) for 24 h and (d) EDS images of sample CA pre-cured for 28 d.

hindered the hydration of cement particles in the later stage [42]. Fig. 11 shows that the particle diameter of fayalite in sample CA had decreased considerably due to dissolution pretreatment [10] and carbonation [8]. The fayalite surface in the uncarbonated and carbonated samples had dissolution stripes [43]. Unhydrated cement particles were observed in sample CA before and after carbonation, explaining why sample CA had the lowest compressive strength among the three samples despite the increase in the continuity of its hardened paste.

The EDS results in Figs. 10 and 11 indicate that under identical carbonation conditions, samples D and CA experienced Al and Ca enrichment on a local scale due to the presence of unhydrated cement particles. Areas with high Mg element contents were also observed in these two samples. The distribution of the Fe element in samples D and CA exhibited a contradictory pattern, with Fe being concentrated in a local area in sample D but being dispersed in sample CA. On the other hand, the distribution of carbon elements in sample D is mainly concentrated inside the pore from Fig. 13.

Figs. 12 and 13 are the EDS results of sample B carbonated at 35 and 80°C for 24 h, respectively. Increasing the carbonation temperature can remarkably increase carbonate content in the hardened paste, as shown by the distribution of carbon elements in Fig. 10. Moreover, areas with high Mg element contents were mainly distributed in the light gray area of the fayalite particle surface. The dissolution and distribution of Mg elements on the paste surface increased with the increase in carbonation temperature.

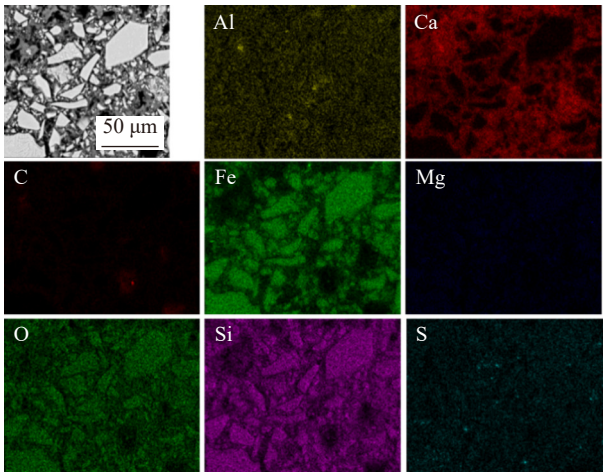

Fig. 12. EDS images of sample B (subjected to 28 d of water curing) carbonated at 35°C for 24 h.

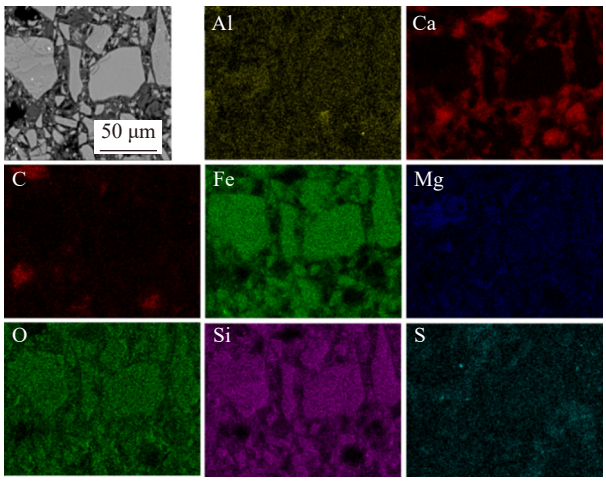

Fig. 13. EDS images of sample B (subjected to 28 d of water curing) carbonated at 80°C for 24 h (carbonates are observed inside the pore areas).

4. Implications

Existing studies state that the main reactants in the carbonation of conventional cement materials are alkali metal hydroxides, free alkali metal oxides, and alkali metal silicate minerals. They include $Ca(OH)_2$, CaO, MgO calcium silicate hydrates (C–S–H) and calcium silicate minerals. They react with CO_2 to form their corresponding metal carbonates [44]. The main carbonation reaction mechanisms in cement are as follows:

$$Ca(OH)_2 + CO_2 \rightarrow CaCO_3 + H_2O \quad (4)$$

$$C-S-H + CO_2 \rightarrow CaCO_3 + H_2O + SiO_2 \quad (5)$$

$$Ca_xSiO_4 + CO_2 + H_2O \rightarrow CaCO_3 + H_2O + SiO_2 \quad (6)$$

Currently, industrial solid wastes, e.g., steel slag, have been widely studied for carbon storage. This is mainly because they have high contents of alkali metal oxides or calcium silicate minerals [45]. These raw materials can react with CO_2 and form carbonates that have certain cementitious and mechanical properties. Their main carbonation reaction mechanisms are as follows:

$$CaO + CO_2 \rightarrow CaCO_3 \quad (7)$$

$$MgO + CO_2 \rightarrow MgCO_3 \quad (8)$$

$$Ca_xSiO_4 + CO_2 + H_2O \rightarrow CaCO_3 + H_2O + SiO_2 \quad (9)$$

CNCM contains olivine minerals, $Ca(OH)_2$, C–S–H gel, and other products produced via cement hydration, as well as some clinker minerals. The olivine phase releases metal cations in CNCM by dissolving the alkaline minerals that are produced by admixtures or cement hydration. These cations then react with CO_2 to form the corresponding carbonates under certain humidity conditions. These carbonates fill pores and improve the macro-performance of CNCM. The main CO_2 mineralization reactions are as follows:

$$Ca(OH)_2 + CO_2 \rightarrow CaCO_3 + H_2O \quad (10)$$

$$C-S-H + CO_2 \rightarrow CaCO_3 + H_2O + SiO_2 \quad (11)$$

$$Ca_xSiO_4 + CO_2 + H_2O \rightarrow CaCO_3 + H_2O + SiO_2 \quad (12)$$

$$Mg_2SiO_4 + CO_2 + H_2O \rightarrow MgCO_3 + H_2O + SiO_2 \quad (13)$$

In previous studies, steel slag is often regarded as industrial waste with the best CO_2 curing performance. Its high CO_2 mineralization capacity is reflected by its calcium content of 25wt%–45wt%. Relevant studies have stated that CO_2 ab-

sorption by steel slag reaches 13.2% after 3 h of carbonization at room temperature [45]. However, CNCM samples have a CAC of only 8.51wt% and are more difficult to carbonate than steel slag. Nevertheless, copper-nickel slag is at least half the price of steel slag and has high carbonation potential. Different carbonated solid wastes should be applied in accordance with their cost performance. CO_2 mineralization is currently one of the most promising methods for reducing CO_2 emissions effectively. The abundance of alkaline silicates in mine tailings and slags can offer a favorable prospect for the direct mineralization of CO_2, which is likely to play a leading role in the coming decades. CNCM samples can be directly studied to evaluate the compatibility of CO_2 mineralization. However, the cost of the activation method should be reduced from the perspective of industrialization [46]

5. Conclusions

This work investigated the potential of olivine-containing copper–nickel slag for CO_2 mineralization in cementitious materials. The carbonation products, CO_2 adsorption amounts, mass variations, mechanical properties, and microstructures of the carbonated CNCM samples were examined. The following conclusions can be drawn on the basis of the results.

(1) TG–DSC results revealed that high temperature, i.e., 80°C in this work, was beneficial to CO_2 adsorption in different activated types of CNCM samples subjected to 3 d of water curing instead of 28 d of water curing. In this case, extending the CO_2 curing time further increased the CO_2 mineralization content. Under these specific carbonation conditions of 80°C and 72 h, the samples that were not subjected to chemical pretreatment after 3 d of water curing exhibited the highest CO_2 adsorption amount of 8.51wt% with the compressive strength of the 39.07 MPa, which indicated that 1 t of this copper-nickel slag composite cementitious material can sequester 85.1 kg of CO_2.

(2) The strength of the samples subjected to 28 d of water pre-curing without chemical pretreatment (Sample B) reached 57.44 MPa when carbonated at 80°C for 24 h. This sample had the highest compressive strength among all the studied samples. Under the same carbonation conditions, the addition of CA was beneficial to CO_2 diffusion and the adsorption amount but had no remarkable positive effect on strength development. The sodium silicate samples presented high strength during the first 3 d of carbonation, and their strength after 28 d of carbonation was second only to that of samples without chemical pretreatment.

(3) XRD demonstrated that the chemical activation methods and carbonation temperature were the main factors affecting $CaCO_3$ polymorphs during carbonation. The samples that did not undergo any chemical pretreatment and those that were activated with water glass showed promising results in the formation of calcite, aragonite and vaterite.

(4) MIP and BSE analyses showed that after carbonation, the admixture-treated samples presented a reduction in total porosity and a considerable improvement in microstructure continuity compared with the untreated samples. The carbonation temperature played a crucial role in modifying the main peak value of pore size distribution. A shift toward larger regions occurred at 35°C, and toward smaller regions occurred at 80°C when compared to the uncarbonated samples.

This work also demonstrated that choosing reasonable activators and modifying the cement hydration degree were the main techniques for accelerating CO_2 diffusion, thus improving the CO_2 adsorption amount in cementitious materials. However, the carbonation of the mature hardened paste at high temperatures (i.e., 80°C) resulted in a loss in compressive strength. In addition, aragonite has higher Mohs hardness than calcite and can fill pores easily with small particle sizes at high pH values, thus increasing the compressive strength of cementitious materials. Moreover, as the carbonation temperature increased, the carbonation and hydration of clinkers progressed synergistically, the content of carbonation products increased, and the degree of hydration intensified. This phenomenon not only increased carbon sequestration but also improved strength and reduced porosity.

Acknowledgements

This work was financially supported by the Intergovernmental International Science and Technology Innovation Cooperation Key Project of the National Key Research and Development Program of China (No. 2022YFE0135100), the National Natural Science Foundation of China (No. 52072171), the Beijing Nova Program (No. 20220484057), and the Priority Academic Program Development of Jiangsu Higher Education Institutions (PAPD).

Conflict of Interest

The authors declare that they have no known competing financial interests or personal relationships that could have appeared to influence the work reported in this paper.

Supplementary Information

The online version contains supplementary material at https://doi.org/10.1007/s12613-023-2743-1.

References

[1] IEA (2023), *CO_2 Emissions in 2022*, IEA, Paris [2022-4-24]. https://www.iea.org/reports/co2-emissions-in-2022

[2] Z. Liu, Z. Deng, S.J. Davis, C. Giron, and P. Ciais, Monitoring global carbon emissions in 2021, *Nat. Rev. Earth Environ.*, 3(2022), No. 4, p. 217.

[3] L.M. Alsarhan, A.S. Alayyar, N.B. Alqahtani, and N.H. Khdary, Circular carbon economy (CCE): A way to invest CO_2 and protect the environment, A review, *Sustainability*, 13(2021), No. 21, art. No. 11625.

[4] S.Y. Pan, Y.H. Chen, L.S. Fan, *et al*., CO_2 mineralization and utilization by alkaline solid wastes for potential carbon reduction, *Nat. Sustain.*, 3(2020), No. 5, p. 399.

[5] G. Gadikota, Carbon mineralization pathways for carbon capture, storage and utilization, *Commun. Chem.*, 4(2021), No. 1, art. No. 23.
[6] J.J. Li and M. Hitch, Ultra-fine grinding and mechanical activation of mine waste rock using a high-speed stirred mill for mineral carbonation, *Int. J. Miner. Metall. Mater.*, 22(2015), No. 10, p. 1005.
[7] Q.F. Guo, X. Xi, S.T. Yang, and M.F. Cai, Technology strategies to achieve carbon peak and carbon neutrality for China's metal mines, *Int. J. Miner. Metall. Mater.*, 29(2022), No. 4, p. 626.
[8] B. Traynor, C. Mulcahy, H. Uvegi, T. Aytas, N. Chanut, and E.A. Olivetti, Dissolution of olivines from steel and copper slags in basic solution, *Cem. Concr. Res.*, 133(2020), art. No. 106065.
[9] E.H. Oelkers, J. Declercq, G.D. Saldi, S.R. Gislason, and J. Schott, Olivine dissolution rates: A critical review, *Chem. Geol.*, 500(2018), p. 1.
[10] C.C. Sun, Z.Q. Yao, Q.Q. Wang, L.J. Guo, and X.D. Shen, Theoretical study on the organic acid promoted dissolution mechanism of forsterite mineral, *Appl. Surf. Sci.*, 614(2023), art. No. 156063.
[11] O. Qafoku, L. Kovarik, R.K. Kukkadapu, *et al*., Fayalite dissolution and siderite formation in water-saturated supercritical CO_2, *Chem. Geol.*, 332-333(2012), p. 124.
[12] D.E. Giammar, R.G. Bruant, and C.A. Peters, Forsterite dissolution and magnesite precipitation at conditions relevant for deep saline aquifer storage and sequestration of carbon dioxide, *Chem. Geol.*, 217(2005), No. 3-4, p. 257.
[13] N.C. Johnson, B. Thomas, K. Maher, R.J. Rosenbauer, D. Bird, and G.E. Brown Jr, Olivine dissolution and carbonation under conditions relevant for *in situ* carbon storage, *Chem. Geol.*, 373(2014), p. 93.
[14] M. Azadi, M. Edraki, F. Farhang, and J. Ahn, Opportunities for mineral carbonation in Australia's mining industry, *Sustainability*, 11(2019), No. 5, art. No. 1250.
[15] A.A. Olajire, A review of mineral carbonation technology in sequestration of CO_2, *J. Petrol. Sci. Eng.*, 109(2013), p. 364.
[16] Z.M. Chen, R. Li, X.M. Zheng, and J.X. Liu, Carbon sequestration of steel slag and carbonation for activating RO phase, *Cem. Concr. Res.*, 139(2021), art. No. 106271.
[17] L.W. Mo and D.K. Panesar, Effects of accelerated carbonation on the microstructure of Portland cement pastes containing reactive MgO, *Cem. Concr. Res.*, 42(2012), No. 6, p. 769.
[18] L. Wang, L. Chen, J.L. Provis, D.C.W. Tsang, and C.S. Poon, Accelerated carbonation of reactive MgO and Portland cement blends under flowing CO_2 gas, *Cem. Concr. Compos.*, 106(2020), art. No. 103489.
[19] S.A. Novikova, Fayalite from Fe-rich paralavas of ancient coal fires in the Kuzbass, Russia, *Geol. Ore Depos.*, 51(2009), No. 8, p. 800.
[20] J.S. Loring, Q.R.S. Miller, C.J. Thompson, and H.T. Schaef, Experimental studies of reactivity and transformations of rocks and minerals in water-bearing supercritical CO_2, [in] *Science of Carbon Storage in Deep Saline Formations*, Elsevier, Amsterdam, 2019, p. 63.
[21] A.T.M. Marsh, T. Yang, S. Adu-Amankwah, and S.A. Bernal, Utilization of metallurgical wastes as raw materials for manufacturing alkali-activated cements, [in] *Waste and Byproducts in Cement-based Materials*, Woodhead Publishing, Sawston, 2021, p. 335.
[22] T. Yang, X. Yao, and Z.H. Zhang, Geopolymer prepared with high-magnesium nickel slag: Characterization of properties and microstructure, *Constr. Build. Mater.*, 59(2014), p. 188.
[23] T. Yang, Z.H. Zhang, H.J. Zhu, X. Gao, C.D. Dai, and Q.S. Wu, re-examining the suitability of high magnesium nickel slag as precursors for alkali-activated materials, *Constr. Build. Mater.*, 213(2019), p. 109.
[24] Y.D. Huang, Q. Wang, and M.X. Shi, Characteristics and reactivity of ferronickel slag powder, *Constr. Build. Mater.*, 156(2017), p. 773.
[25] C.L. Wang, Z.Z. Ren, Z.K. Huo, *et al*., Properties and hydration characteristics of mine cemented paste backfill material containing secondary smelting water-granulated nickel slag, *Alex. Eng. J.*, 60(2021), No. 6, p. 4961.
[26] T. Yang, Z.H. Zhang, Q. Wang, and Q.S. Wu, ASR potential of nickel slag fine aggregate in blast furnace slag–fly ash geopolymer and Portland cement mortars, *Constr. Build. Mater.*, 262(2020), art. No. 119990.
[27] F. Wang, D. Dreisinger, M. Jarvis, and T. Hitchins, Kinetics and mechanism of mineral carbonation of olivine for CO_2 sequestration, *Miner. Eng.*, 131(2019), p. 185.
[28] F. Wang, D. Dreisinger, M. Jarvis, T. Hitchins, and L. Trytten, CO_2 mineralization and concurrent utilization for nickel conversion from nickel silicates to nickel sulfides, *Chem. Eng. J.*, 406(2021), art. No. 126761.
[29] Z.Q. Yao, C.C. Sun, Q.Q. Wang, and X.D. Shen, The dissolution kinetics of copper–nickel slag, [in] *the 10th International Symposium on Cement and Concrete* (*ISCC 2022*), Guangzhou, 2022, p. 14.
[30] P. Giannaros, A. Kanellopoulos, and A. Al-Tabbaa, Sealing of cracks in cement using microencapsulated sodium silicate, *Smart Mater. Struct.*, 25(2016), No. 8, art. No. 084005.
[31] E. Drouet, S. Poyet, P. Le Bescop, J.M. Torrenti, and X. Bourbon, Carbonation of hardened cement pastes: Influence of temperature, *Cem. Concr. Res.*, 115(2019), p. 445.
[32] Y.X. Zhao, F. Wei, and Y. Yu, Effects of reaction time and temperature on carbonization in asphaltene pyrolysis, *J. Petrol. Sci. Eng.*, 74(2010), No. 1-2, p. 20.
[33] N. Wada, K. Kanamura, and T. Umegaki, Effects of carboxylic acids on the crystallization of calcium carbonate, *J. Colloid Interface Sci.*, 233(2001), No. 1, p. 65.
[34] Y.F. Ma, Y.H. Gao, and Q.L. Feng, Effects of pH and temperature on $CaCO_3$ crystallization in aqueous solution with water soluble matrix of pearls, *J. Cryst. Growth*, 312(2010), No. 21, p. 3165.
[35] M. Kogo, K. Suzuki, T. Umegaki, and Y. Kojima, Control of aragonite formation and its crystal shape in $CaCl_2$–Na_2CO_3–H_2O reaction system, *J. Cryst. Growth*, 559(2021), art. No. 125964.
[36] S.L. Guo, Y. Lu, Y.H. Bu, and B.L. Li, Effect of carboxylic group on the compatibility with retarder and the retarding side effect of the fluid loss control additive used in oil well cement, *R. Soc. Open Sci.*, 5(2018), No. 9, art. No. 180490.
[37] X.H. Ye, T.W. Chen, and J.K. Chen, Carbonation of cement paste under different pressures, *Constr. Build. Mater.*, 370(2023), art. No. 130511.
[38] F. Matsushita, Y. Aono, and S. Shibata, Calcium silicate structure and carbonation shrinkage of a tobermorite-based material, *Cem. Concr. Res.*, 34(2004), No. 7, p. 1251.
[39] V.W.Y. Tam, A. Butera, and K.N. Le, An investigation of the shrinkage, concrete shrinkage reversibility and permeability of CO_2-treated concrete, *Constr. Build. Mater.*, 365(2023), art. No. 130120.
[40] Q.S. Chen, L.M. Zhu, Y.M. Wang, J. Chen, and C.C. Qi, The carbon uptake and mechanical property of cemented paste backfill carbonation curing for low concentration of CO_2, *Sci. Total Environ.*, 852(2022), art. No. 158516.
[41] X. Luo, S.J. Li, Z.H. Guo, C. Liu, and J.M. Gao, Effect of curing temperature on the hydration property and microstructure of Portland cement blended with recycled brick powder, *J. Build.*

Eng., 61(2022), art. No. 105327.
[42] M. Mejdi, W. Wilson, M. Saillio, T. Chaussadent, L. Divet, and A. Tagnit-Hamou, Hydration and microstructure of glass powder cement pastes—A multi-technique investigation, *Cem. Concr. Res.*, 151(2022), art. No. 106610.
[43] X.D. Li, Q.Q. Wang, X.D. Shen, E.T. Pedrosa, and A. Luttge, Multiscale investigation of olivine (010) face dissolution from a surface control perspective, *Appl. Surf. Sci.*, 549(2021), art. No. 149317.
[44] M. Kazemian and B. Shafei, Carbon sequestration and storage in concrete: A state-of-the-art review of compositions, methods, and developments, *J. CO_2 Util.*, 70(2023), art. No. 102443.
[45] P. Liu, L.W. Mo, and Z. Zhang, Effects of carbonation degree on the hydration reactivity of steel slag in cement-based materials, *Constr. Build. Mater.*, 370(2023), art. No. 130653.
[46] F. Wang and D. Dreisinger, Status of CO_2 mineralization and its utilization prospects, *Miner. Miner. Mater.*, 1(2022), art. No. 4.